Suppression of Donor-Driven Spin Relaxation in Strained $Si_{0.1}Ge_{0.9}$

T. Naito,[1] M. Yamada[ORCID],[2] S. Yamada,[1,2] K. Sawano,[3] and K. Hamaya[ORCID][1,2,*]

[1]*Department of Systems Innovation, Graduate School of Engineering Science, Osaka University, 1-3 Machikaneyama, Toyonaka, 560-8531, Japan*

[2]*Center for Spintronics Research Network, Graduate School of Engineering Science, Osaka University, 1-3 Machikaneyama, Toyonaka, 560-8531, Japan*

[3]*Advanced Research Laboratories, Tokyo City University, 8-15-1 Todoroki, Tokyo, 158-0082, Japan*

We experimentally study the strain effect on electron spin relaxation in a semiconductor using nonlocal spin-transport measurements in lateral spin-valve devices. Application of in-plane and biaxial tensile strain to a (111)-oriented and heavily doped *n*-type $Si_{0.1}Ge_{0.9}$ layer leads to lifting of the valley degeneracy in the conduction band and to reduction of the electron's effective mass, resulting in increased electron mobility. Nonlocal four-terminal spin signals in the strained-$Si_{0.1}Ge_{0.9}$ lateral spin-valve devices are markedly enhanced and the estimated spin lifetime becomes 3 times longer than that in strain-free devices at low temperatures. On the basis of a comparison of the experimental data and recent theories, we propose that only the donor-driven intervalley spin-flip scattering of electrons at low temperatures is partly suppressed for the strained and heavily doped $Si_{0.1}Ge_{0.9}$.

I. INTRODUCTION

Use of the spin degree of freedom in semiconductors has been explored for next-generation electronics with low power consumption [1–5]. To demonstrate spin-based logic and memory architectures [6,7], researchers have investigated electrical spin injection, transport, detection, and spin relaxation in gallium arsenide (GaAs) [8–11], graphene [12–14], silicon (Si) [15–20], and germanium (Ge) [21–25]. In particular, general group-IV semiconductors such as Si and Ge are expected to transport long-lived spin information because of their large spin diffusion length and long spin lifetime, which are consequences of their weak spin-orbit coupling and lattice inversion symmetry in the crystal structure [26–30]. A long spin-transport length of electrons has been detected electrically for intrinsic Si [15,16] and Ge [31]. Because of the optically accessible nature of the conduction-band structures in intrinsic and lightly doped Ge, relatively-long-lived spin information in Ge was also confirmed by optical methods [32–37].

Recently, for intrinsic Si and Ge, the spin relaxation of electrons has been theoretically suggested to be dominated mainly by the electron-phonon interaction inducing spin-flip transitions between the degenerate multivalley conduction bands (i.e., intervalley spin-flip scattering) [27–30]. In addition, for impurity-doped Si and Ge, Song *et*

al. [38] theoretically proposed that the dominant spin-relaxation mechanism is intervalley spin-flip scattering induced by the central-cell potential of impurities—so-called donor-driven spin relaxation—where its origin is the short-range spin scattering because of the spin-orbit coupling of impurities rather than the spin mixing of states from the spin-orbit coupling in the host Si and Ge. The phonon-induced and impurity-induced intervalley spin-flip scattering mechanisms were subsequently verified even in experimental studies on lateral spin transport in doped Si [18,39] and doped Ge [24,25,40]. As a result of the remarkable aforementioned progress toward understanding the electron spin-relaxation mechanism for Si and Ge, the intervalley-spin-flip-scattering process in Si or Ge devices can be controlled by lifting the valley degeneracy in the conduction band [29,30,41].

Here we report an experimental demonstration of suppressing the spin relaxation of electrons at low temperatures using nonlocal spin-transport measurements in lateral spin-valve (LSV) devices with a strained $Si_{0.1}Ge_{0.9}$(111) layer. Notably, we use $Si_{0.1}Ge_{0.9}$ as a spin-transport layer because the electronic band structure of $Si_{0.1}Ge_{0.9}$ is similar to that of Ge and because effective in-plane and biaxial tensile strain can be induced by forming a high-quality $Si_{0.1}Ge_{0.9}$/Ge(111) heterostructure [42–44]. On lifting the valley degeneracy of the conduction band and reducing the electron's effective mass, we observe an increase in electron mobility in the strained $Si_{0.1}Ge_{0.9}$. Nonlocal four-terminal spin signals in the strained-$Si_{0.1}Ge_{0.9}$ devices

are markedly enhanced and are as much as 2 orders of magnitude larger than those in strain-free-$Si_{0.1}Ge_{0.9}$ devices at low temperatures. From the nonlocal Hanle analysis, we experimentally find that the spin lifetime at low temperatures can be extended to as much as 3 times that in the strain-free devices. We propose that only the donor-driven intervalley spin-flip scattering of electrons is partly suppressed for the strained $Si_{0.1}Ge_{0.9}$.

II. RESULTS AND DISCUSSION

A. Growth and characterization of strained $Si_{0.1}Ge_{0.9}(111)$

To control the spin relaxation of electrons in the degenerate conduction-band valleys, we use a strain-induced $Si_{0.1}Ge_{0.9}(111)$ spin-transport layer, where the composition of $Si_{0.1}Ge_{0.9}$ is known to maintain a Ge-like electronic band structure in which the bottom of the conduction band is located near the L point in the **k** space [42,43]. Figures 1(a) and 1(b) show a schematic and cross-section-transmission-electron-microscopy images, respectively, of the $Si_{0.1}Ge_{0.9}(111)$ layer grown on a Ge(111)/Si(111) substrate. Using molecular beam epitaxy (MBE), we first form an undoped Ge(111) layer (40 nm) grown at $350\,^{\circ}C$ [low-temperature (LT) Ge layer] on an undoped Si(111) substrate ($\rho \sim 1000\ \Omega cm$) and then form an undoped Ge(111) layer (600 nm) grown at $700\,^{\circ}C$ [high-temperature (HT) Ge layer] [46,47]. As shown at the bottom of Fig. 1(b), the defects from the Si(111) substrate are stopped in the HT Ge layer. We next grow an 80-nm-thick phosphorus (P)-doped n-type $Si_{0.1}Ge_{0.9}(111)$ layer by MBE at $350\,^{\circ}C$ on the defect-free surface of the HT Ge layer. For the Schottky-tunnel conduction of electrons in spin-transport measurements, we grow an 8-nm-thick P δ-doped Ge layer with an ultrathin Si layer on top of the spin-transport layer [48], as shown at the top of Fig. 1(b). As a consequence, we have already established reliable spin-transport measurements in Ge-based LSV devices with Schottky-tunnel contacts [4]. As a reference, we also prepare a strain-free $Si_{0.1}Ge_{0.9}$ layer, as described in Refs. [45,49], where the thickness of the HT Ge layer is 70 nm and there are lots of defects originating from misfit dislocations at the LT Ge/Si(111) interface, giving rise to the release of the lattice strain in the $Si_{0.1}Ge_{0.9}$ layer.

Figure 1(c) displays x-ray-diffraction ω-2θ scan data for the newly grown $Si_{0.1}Ge_{0.9}$. A clear $Si_{0.1}Ge_{0.9}(333)$ peak with interference fringes is observed, indicating coherent and epitaxial growth of the $Si_{0.1}Ge_{0.9}$ layer on the Ge(111)/Si(111) substrate. Because the lattice constant of the newly grown $Si_{0.1}Ge_{0.9}$ layer is compressed along the [111] direction, an in-plane and biaxial tensile strain is applied to the $Si_{0.1}Ge_{0.9}$ layer. The presence of the lattice strain in the $Si_{0.1}Ge_{0.9}$ layer is confirmed by x-ray-diffraction reciprocal-space-map measurements (not shown here). When the in-plane and biaxial tensile strain
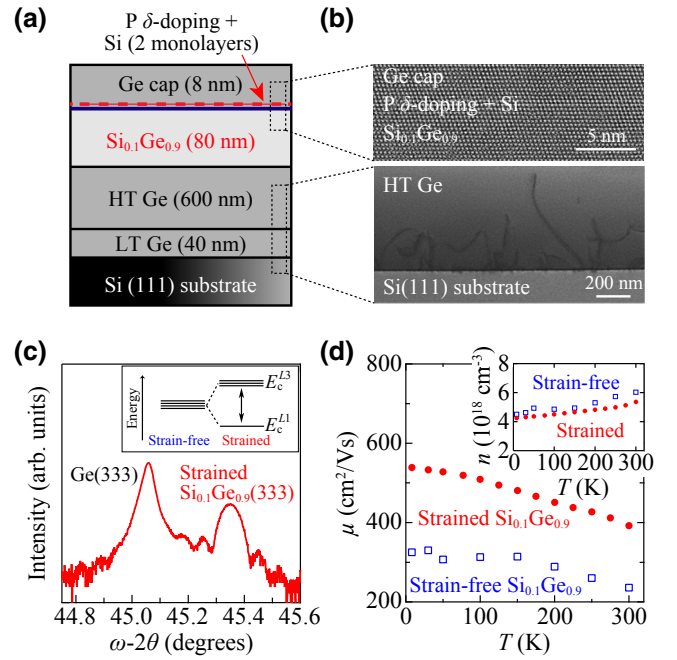

FIG. 1. (a) Schematic and (b) cross-section-transmission-electron-microscopy images of the grown $Si_{0.1}Ge_{0.9}$/Ge/Si(111) heterostructure for spin-transport measurements of the strained $Si_{0.1}Ge_{0.9}$. (c) X-ray-diffraction rocking curve around the Ge(333) peak for the strained $Si_{0.1}Ge_{0.9}$ layer on the Ge/Si(111) virtual substrate. The inset shows a schematic of the energy splitting of the conduction-band valleys in $Si_{0.1}Ge_{0.9}$. (d) μ-T plots of the grown strained $Si_{0.1}Ge_{0.9}$ layer and strain-free $Si_{0.1}Ge_{0.9}$ layer, as reported in Ref. [45]. The inset shows n-T plots for both the strained $Si_{0.1}Ge_{0.9}$ layer and the strain-free $Si_{0.1}Ge_{0.9}$ layer.

is coherently applied, the four degenerate L valleys of the conduction band in $Si_{0.1}Ge_{0.9}$ can be lifted to a single low-energy valley E_c^{L1} and three higher-energy valleys E_c^{L3} [30,50,51], as illustrated in the inset in Fig. 1(c). From the literature [50,51], the energy splitting for $Si_{0.1}Ge_{0.9}$ grown coherently on Ge(111) is expected to be 55–90 meV.

The carrier concentration (n) in both the strained $Si_{0.1}Ge_{0.9}$ layer and the strain-free $Si_{0.1}Ge_{0.9}$ layer is determined from Hall-effect measurements to be approximately 5.4×10^{18} and 6.0×10^{18} cm^{-3}, respectively, at room temperature; the temperature dependence of n is shown in the inset in Fig. 1(d). Figure 1(d) shows the temperature dependence of the electron mobility (μ) for both the strained $Si_{0.1}Ge_{0.9}$ layer and the strain-free $Si_{0.1}Ge_{0.9}$ layer. After the strain is applied to the $Si_{0.1}Ge_{0.9}$ layer, the electron mobility is clearly increased from approximately 240 cm^2/Vs to approximately 390 cm^2/Vs at room temperature. Notably, even in the low-temperature regime from 8 to 100 K, the electron mobility is further increased to approximately 540 cm^2/Vs despite the presence of the heavy doping of P impurity in the spin-transport layer. This feature indicates that the increase of the electron mobility

arises from the suppression of the impurity-induced inter-valley momentum scattering of electrons and the reduction in the electron's effective mass in the strained $Si_{0.1}Ge_{0.9}$ [44,52–54].

B. Spin transport in strained $Si_{0.1}Ge_{0.9}$

To examine the spin transport in the strained $Si_{0.1}Ge_{0.9}$, we fabricate LSV devices with various center-to-center distances d between the spin injector and the detector, as shown in Fig. 2(a). Details of the fabrication processes and top views of similar LSV devices have been reported elsewhere [4,55]. As a spin injector and detector, we grow $Co_2FeAl_xSi_{1-x}$ (CFAS), which is a highly-spin-polarized Heusler alloy [56,57], by MBE on top of the Schottky-tunnel barriers using nonstoichiometric growth techniques [4,25]. As depicted in Fig. 2(a), four-terminal nonlocal voltage measurements are performed at various temperatures [4,8,58,59]. Figure 2(b) shows a representative non-local spin signal [$\Delta R_{NL} = \Delta V_{NL}/I = (V_{NL}^{\uparrow\downarrow} - V_{NL}^{\uparrow\uparrow})/I$] of a LSV device with a strained $Si_{0.1}Ge_{0.9}$ layer (device A; $d = 2.2$ μm) at 77 K. Here in-plane magnetic fields (B_y) are applied along the y direction and the spin-polarized electrons are injected into the $Si_{0.1}Ge_{0.9}$ from the CFAS for a negative value of I ($I < 0$) (spin-injection conditions). Hysteretic features are observed, where the changes in ΔR_{NL} depend on the magnetization states between parallel and antiparallel. Notably, the magnitude of ΔR_{NL} for the strained $Si_{0.1}Ge_{0.9}$ is 2 orders of magnitude larger than

that for the strain-free $Si_{0.1}Ge_{0.9}$ reported in Ref. [45]. When LSV devices are fabricated again with the strain-free $Si_{0.1}Ge_{0.9}$ and nonlocal measurements at 77 K are performed, 2-order-smaller ΔR_{NL} data are obtained for the strain-free LSV devices. Thus, the great increase in ΔR_{NL} is related to the application of the in-plane and biaxial tensile strain to the $Si_{0.1}Ge_{0.9}$ spin-transport layer.

As shown in Fig. 2(c), Hanle-type spin-precession signals are observed when out-of-plane magnetic fields (B_z) are applied under parallel and antiparallel magnetization states. Here, for clarity, we subtract a quadratic background from the raw data [4,8]. The nonlocal spin-valve and Hanle signals indicate that reliable spin transport in the strained $Si_{0.1}Ge_{0.9}$ is demonstrated experimentally. Notably, even at 77 K, B_z for the spin dephasing is small compared with that for the strain-free $Si_{0.1}Ge_{0.9}$ [45]. To verify the reproducibility of the measurements, Hanle curves for the parallel magnetization state at 50 K are recorded for numerous LSV devices with the strained $Si_{0.1}Ge_{0.9}$; the results are reported in Fig. 3, where two of the measured LSV devices are labeled as device B ($d = 1.4$ μm) and device C ($d = 2.2$ μm). As a reference, the Hanle curve for a LSV device with the strain-free $Si_{0.1}Ge_{0.9}$ at 50 K is also shown. The Hanle curves for devices B and C with the strained $Si_{0.1}Ge_{0.9}$ are narrow compared with the curve for the devices with strain-free $Si_{0.1}Ge_{0.9}$.

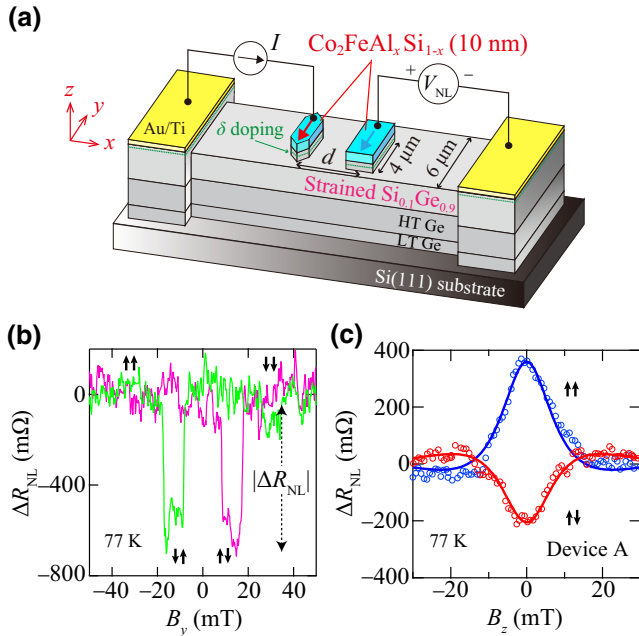From these Hanle curves and the following equation [8,59], we can extract the spin lifetime (τ_N), together with

FIG. 2. (a) Schematic of the fabricated CFAS/strained-$Si_{0.1}Ge_{0.9}$-based LSV device. (b) Nonlocal spin signal and (c) nonlocal Hanle curves for parallel and antiparallel magnetization states of a strained-$Si_{0.1}Ge_{0.9}$ device at 77 K.
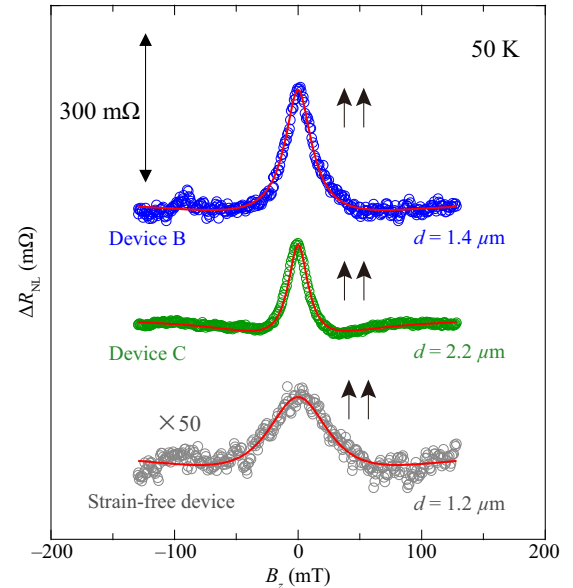

FIG. 3. Hanle curves for various strained $Si_{0.1}Ge_{0.9}$ layers measured in the parallel magnetization state at 50 K. As a reference, an enlarged Hanle curve for a strain-free $Si_{0.1}Ge_{0.9}$ layer at 50 K is shown.

the diffusion constant (D):

$$\Delta R_{\mathrm{NL}}(B_z) = \pm A \int_0^\infty \phi(t)\cos(\omega_L t)\exp\left(-\frac{t}{\tau_N}\right)dt, \quad (1)$$

where $A = P_{\mathrm{inj}}P_{\mathrm{det}}\rho_N D/S$, $\phi(t) = (1/\sqrt{4\pi Dt})\exp\left(-d^2/4Dt\right)$, and $\omega_L (= g\mu_B B_z/\hbar)$ is the Larmor frequency, where g is the electron g factor ($g = 1.56$) in $Si_{0.1}Ge_{0.9}$ [51,60] and μ_B is the Bohr magneton. P_{inj} and P_{det} are spin polarizations of the electrons in $Si_{0.1}Ge_{0.9}$ created by the spin injector and detector, respectively. ρ_N and S are the resistivity (approximately 2.7 mΩcm) and the cross-section area (0.48 μm^2) of the $Si_{0.1}Ge_{0.9}$ layer, respectively. Here the contact-induced spin relaxation does not influence the Hanle analysis [61] because the resistance-area product of these LSV devices is 1 order of magnitude larger than the spin resistance of the $Si_{0.1}Ge_{0.9}$ layer. We fit the data for devices B and C, which have strained $Si_{0.1}Ge_{0.9}$ layers, using Eq. (1) and can extract τ_N at 50 K of approximately 0.68 ns and approximately 0.83 ns, respectively, where the D values obtained are approximately 37 cm^2/s and approximately 41 cm^2/s, respectively. By contrast, for the strain-free $Si_{0.1}Ge_{0.9}$ in this study and in a previous study [45], τ_N at 50 K is estimated to be approximately 0.2 ns ($D = 11$–17 cm^2/s). From these results, we conclude that the τ_N values for the strained $Si_{0.1}Ge_{0.9}$ are greater than those for the strain-free $Si_{0.1}Ge_{0.9}$. In this case, we also obtain the spin diffusion length (λ_N) of the spin-transport layer from the relation $\lambda = \sqrt{D\tau}$. λ_N for the strained $Si_{0.1}Ge_{0.9}$ is 1.6–1.9 μm, which is approximately 3 times greater than that (0.5–0.6 μm) for the strain-free $Si_{0.1}Ge_{0.9}$. This phenomenon is consistent with the increase in μ shown in Fig. 1(d) for the strained $Si_{0.1}Ge_{0.9}$ because λ_N is generally influenced by the value of μ related to D [4,18,25].

Figure 4 shows the temperature dependence of τ_N for strained-$Si_{0.1}Ge_{0.9}$ devices A–D, where device D also has $d = 1.4$ μm, together with the temperature dependence of τ_N for the strain-free-$Si_{0.1}Ge_{0.9}$ devices. The estimated τ_N values for strained-$Si_{0.1}Ge_{0.9}$ devices A–D are approximately 3 or 4 times larger than those for the strain-free ones in the temperature range 8 K $\leq T \leq$ 77 K. The aforementioned results provide experimental evidence for suppressing the spin relaxation of electrons through the use of a strained $Si_{0.1}Ge_{0.9}$ spin-transport layer. Above approximately 100 K, however, decreases in τ_N are observed for devices A–D. If the intervalley spin-flip scattering were completely suppressed by lifting the valley degeneracy of the conduction bands, even the decrease in τ_N above approximately 100 K should also be limited, as expected in theory [30]. Thus, in the present study, the temperature dependence of τ_N above approximately 100 K is considered a consequence of an insufficient strain effect on the spin transport. For the strain-free devices, by contrast, reliable τ_N data could not be obtained above approximately
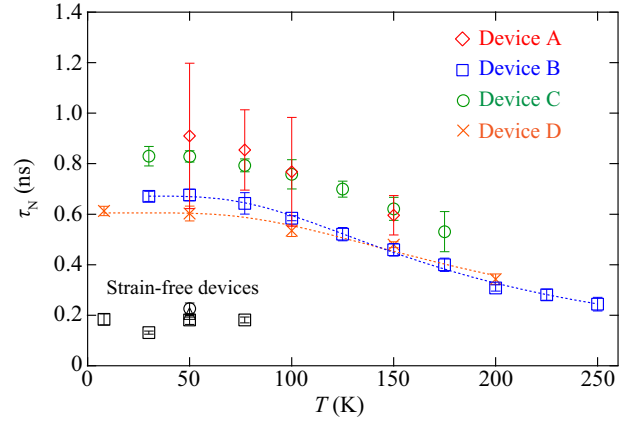

FIG. 4. Temperature dependence of τ_N for various strained-$Si_{0.1}Ge_{0.9}$ LSV devices as estimated from the Hanle curves corresponding to the parallel magnetization state. For comparison, the data for strain-free-$Si_{0.1}Ge_{0.9}$ LSV devices are also plotted.

100 K because of the small ΔR_{NL} value. In the next section, we discuss the spin-relaxation mechanism in the strained $Si_{0.1}Ge_{0.9}$.

C. Spin-relaxation mechanism in strained $Si_{0.1}Ge_{0.9}$

According to Matthiessen's rule, if we consider the impurity-induced and phonon-induced intervalley spin-flip scatterings in the strained $Si_{0.1}Ge_{0.9}$, then the spin scattering rate ($1/\tau_N$) can be expressed as

$$\frac{1}{\tau_N} = \frac{1}{\tau_{\mathrm{imp}}} + \frac{1}{\tau_{\mathrm{phon}}^{\mathrm{inter}}}, \quad (2)$$

where τ_{imp} and $\tau_{\mathrm{phon}}^{\mathrm{inter}}$ are spin lifetimes due to the impurity-induced (donor-driven) [38] and phonon-induced [30] intervalley spin-flip scatterings, respectively. In this case, the component of phonon-induced intravalley spin-flip scattering ($1/\tau_{\mathrm{phon}}^{\mathrm{intra}}$) is negligibly small [18,24,25,30,39,40]. For heavily doped (degenerate) Si, Ge, and Si_xGe_{1-x}, the $1/\tau_{\mathrm{imp}}$ term can generally be regarded as the following equation [38,40]:

$$\frac{1}{\tau_{\mathrm{imp}}} \approx \frac{4\pi n m_e a_B^6}{27\hbar^3}\left(3\pi^2 n\right)^{1/3}\Delta_{\mathrm{SO}}^2, \quad (3)$$

where for $Si_{0.1}Ge_{0.9}$, a_B is the Bohr radius, m_e is the electron effective mass, and Δ_{SO} is the spin–orbit-coupling-induced splitting of the triply degenerate $1s$ (T_2) donor state. In Eq. (3), we assign $\epsilon_F \approx \hbar^2/2m_e\left(3\pi^2 n\right)^{2/3}$ to $\epsilon_{\mathbf{k}}$ in Eq. (4) in Ref. [38]. As described in Eq. (3), the $1/\tau_{\mathrm{imp}}$ term depends not on the external temperature but on n [40]. For both the strain-free $Si_{0.1}Ge_{0.9}$ layer and the strained $Si_{0.1}Ge_{0.9}$ layer, because the temperature dependence of n is small, as shown in the inset in Fig. 1(d), the nearly

constant values of τ_N in the temperature range 8 K $\leq T \leq$ 77 K for each device in Fig. 4 indicate that the impurity-induced intervalley spin-flip scattering is dominant. Above approximately 100 K, however, the onset of the decrease in τ_N reflects the influence of the phonon-induced intervalley spin-flip scattering. Because of the insufficient strain effect on the spin transport in $Si_{0.1}Ge_{0.9}$ above approximately 100 K, we tentatively consider the $1/\tau_{phon}^{inter}$ term as the electron-phonon-induced spin-flip process between conduction valleys as in Ge as follows [30]:

$$\frac{1}{\tau_{phon}^{inter}} = \frac{4}{3}\left(\frac{2m_d}{\pi}\right)^{3/2} \sum_{i=1,4} \frac{A_i D_{X_i}^2}{\hbar^2 \varrho \sqrt{\Omega_i}} \frac{\vartheta(y_i)}{\exp y_i - 1}, \quad (4)$$

where m_d, ϱ, and A_i are the effective electron mass in bulk Ge, the crystal density, and the spin-orientation-related constants, respectively, Ω_i is the energy of X-point zone-edge phonons (X_1 and X_4), $\vartheta(y_i = \Omega_i/k_B T) = \sqrt{y_i} \exp(y_i/2) K_{-1}(y_i/2)$ is related to the modified Bessel function of the second kind, and D_{X_i} is the spin-flip-scattering constant, which can be determined from theoretical calculations or from experiments [30]. Using Eq. (2), we analyze the experimental data in Fig. 4.

Because the error bars of the data are relatively large and clear data cannot be obtained at high temperatures for devices A and C, we conduct the data analysis only for devices B and D. The fitting results corresponding to our attempt to fit the experimental data using Eq. (2) with τ_{imp}, D_{X_1}, and D_{X_4} of Eq. (4) as fitting parameters are indicated as the dashed curves in Fig. 4; the extracted parameters τ_{imp}, D_{X_1}, and D_{X_4} are shown in Table I. The good fitting results again indicate the presence of strong contributions of the $1/\tau_{phon}^{inter}$ term in addition to the $1/\tau_{imp}$ term. As a result, τ_{imp} for the strained $Si_{0.1}Ge_{0.9}$ is 3 times greater than that for the strain-free $Si_{0.1}Ge_{0.9}$ (approximately 0.2 ns) [45]. However, because the values of D_{X_1} and D_{X_4} obtained are consistent with our previous work on Ge [4,25], we can attribute the temperature dependence of τ_N above approximately 100 K to the phonon-induced intervalley spin-flip scattering of electrons, similarly to the case of Ge. A comparison of the τ_{imp} values in Table I and Eq. (3) enables a rough estimate of Δ_{SO}. According to the literature [42,43,51,52], the a_B and m_e values for $Si_{0.1}Ge_{0.9}$ can be reasonably assumed to be almost equivalent to those for pure Ge. Thus, for the estimate of Δ_{SO}, we tentatively use $a_B = 6.45$ nm [62], $m_e = 0.16m_0$ [63], and $n = 4.4 \times 10^{18}$ cm^{-3} (50 K). Consequently, Δ_{SO} for device B is 0.079 meV and for device D is 0.084 meV. Here the values of Δ_{SO} are generally much smaller than the valley-orbit-induced singlet-triplet splitting in P-doped Ge of approximately 2.83 meV [64]. Differences in the τ_N values are observed among devices A–D despite their similar values of n. We infer that the observed differences in the τ_N values among the devices are due to the fluctuation

TABLE I. Comparison of the extracted parameters from the data analysis with Eq. (2) for devices B and D with strained $Si_{0.1}Ge_{0.9}$.

	Device B	Device D
τ_{imp} (ns)	0.67	0.61
D_{X_1} (meV/Å)	57.9	67.7
D_{X_4} (meV/Å)	131	80.3

of the microscopic strain effect on the spin-transport layer in LSV devices [65–67]. Given the difference in the data in Fig. 4, we interpret this to mean that Δ_{SO} falls in the range from 0.06 to 0.15 meV, which is consistent with the Δ_{SO} values of 0.06–0.11 meV reported in our previous work on P-doped Ge [4,25,40].

Finally, we comment on the suppression of the phonon-induced intervalley spin-flip scattering in the strained Si_xGe_{1-x} above 100 K. As previously mentioned, the energy splitting of the conduction valleys for the strained $Si_{0.1}Ge_{0.9}$ is expected to be 55–90 meV on the basis of the results of the previous theoretical calculations [50,51]. Although the absolute value of the energy splitting, which is greater than approximately 26 meV (300 K), is likely sufficient to suppress the phonon-induced intervalley spin-flip scattering even near room temperature, the experimental data in this study clearly show the strong influence of the $1/\tau_{phon}^{inter}$ term on the spin transport. As one of the possible reasons for the strong influence of the $1/\tau_{phon}^{inter}$ term, we suggest the influence of the position of the Fermi level (E_F) relative to the three higher-energy valleys (i.e., E_c^{L3}) [30,50], as shown in the inset in Fig. 1(c). In this study, because the value of E_F in the degenerate $Si_{0.1}Ge_{0.9}$ is larger than the energy of the conduction-band edge, the position of the Fermi level is located between E_c^{L3} and E_c^{L1} and the relative position between E_F and E_c^{L3} can become smaller than approximately 26 meV. Given the influence on τ_N at approximately 100 K in Fig. 4, we can estimate the energy difference between E_F and E_c^{L3} as being less than approximately 10 meV. Therefore, we should explore the use of nondegenerate spin-transport layers to create a large energy difference between E_F and E_c^{L3}. Here we also compare the data in the present study with the data for pure (strain-free) Ge reported in our previous work [4,25,68]. Although the strain effect discussed here is partly effective at low temperatures for heavily doped $Si_{0.1}Ge_{0.9}$ spin-transport layers, the advantage of the strained $Si_{0.1}Ge_{0.9}$ is not observed for strain-free n-type Ge above 100 K. Because there is almost no strain effect on the spin transport above 100 K in the present study, we infer that the alloy scattering of electrons in the $Si_{0.1}Ge_{0.9}$ layers [44,69] becomes preferentially dominant for the spin relaxation [70]. That is, if the effective strain is not induced in the Si_xGe_{1-x} layers, there is no advantage in using Si_xGe_{1-x} for spintronic applications. According

to the aforementioned results, in addition to the nondegenerate spin-transport layers, Si_xGe_{1-x} ($0.1 \leq x \leq 0.3$) should be used to enhance the in-plane and biaxial tensile strain to suppress the phonon-induced intervalley spin-flip scattering even at room temperature [42,43,51].

III. CONCLUSION

We experimentally study the strain effect on electron-spin relaxation in a heavily doped strained $Si_{0.1}Ge_{0.9}$ layer using nonlocal spin-transport measurements in LSV devices. Lifting the valley degeneracy of the conduction band enabled us to observe an increase in electron mobility in the strained $Si_{0.1}Ge_{0.9}$ layer. Nonlocal four-terminal spin signals in the strained-$Si_{0.1}Ge_{0.9}$ LSV devices are markedly enhanced and the estimated spin lifetime becomes 3 times longer than that in the strain-free devices at low temperatures. A comparison of the experimental data and a recent theoretical prediction [30,38] leads us to propose that only the donor-driven intervalley spin-flip scattering of electrons is partly suppressed for the strained $Si_{0.1}Ge_{0.9}$. Suppressing the phonon-induced intervalley spin-flip scattering of electrons would require further enhancement of the in-plane and biaxial tensile strain and the use of the nondegenerate condition for Si_xGe_{1-x} spin-transport layers.

ACKNOWLEDGMENTS

[1] I. Žutić, J. Fabian, and S. D. Sarma, Spintronics: Fundamentals and applications, Rev. Mod. Phys. **76**, 323 (2004).

[2] A. M. Bratkovsky, Spintronic effects in metallic, semiconductor, metal-oxide and metal-semiconductor heterostructures, Rep. Prog. Phys. **71**, 026502 (2008).

[3] A. Hirohata and K. Takanashi, Future perspectives for spintronic devices, J. Phys. D: Appl. Phys. **47**, 193001 (2014).

[4] K. Hamaya, Y. Fujita, M. Yamada, M. Kawano, S. Yamada, and K. Sawano, Spin transport and relaxation in germanium, J. Phys. D: Appl. Phys. **51**, 393001 (2018).

[5] W. Liu, P. K. J. Wong, and Y. Xu, Hybrid spintronic materials: Growth, structure and properties, Prog. Mater. Sci. **99**, 27 (2019).

[6] H. Dery, P. Dalal, Ł. Cywiński, and L. J. Sham, Spin-based logic in semiconductors for reconfigurable large-scale circuits, Nature (London) **447**, 573 (2007).

[7] M. Tanaka and S. Sugahara, MOS-based spin devices for reconfigurable logic, IEEE Trans. Electron Devices **54**, 961 (2007).

[8] X. Lou, C. Adelmann, S. A. Crooker, E. S. Garlid, J. Zhang, K. S. M. Reddy, S. D. Flexner, C. J. Palmstrøm, and P. A. Crowell, Electrical detection of spin transport in lateral ferromagnet-semiconductor devices, Nat. Phys. **3**, 197 (2007).

[9] M. Ciorga, A. Einwanger, U. Wurstbauer, D. Schuh, W. Wegscheider, and D. Weiss, Electrical spin injection and detection in lateral all-semiconductor devices, Phys. Rev. B **79**, 165321 (2009).

[10] T. A. Peterson, S. J. Patel, C. C. Geppert, K. D. Christie, A. Rath, D. Pennachio, M. E. Flatté, P. M. Voyles, C. J. Palmstrøm, and P. A. Crowell, Spin injection and detection up to room temperature in Heusler alloy/*n*-GaAs spin valves, Phys. Rev. B **94**, 235309 (2016).

[11] Z. Lin, D. Pan, M. Rasly, and T. Uemura, Electrical spin injection into AlGaAs/GaAs-based two-dimensional electron gas systems with Co_2MnSi spin source up to room temperature, Appl. Phys. Lett. **114**, 012405 (2019).

[12] N. Tombros, C. Jozsa, M. Popinciuc, H. T. Jonkman, and B. J van Wees, Electronic spin transport and spin precession in single graphene layers at room temperature, Nature (London) **448**, 571 (2007).

[13] T.-Y. Yang, J. Balakrishnan, F. Volmer, A. Avsar, M. Jaiswal, J. Samm, S. R. Ali, A. Pachoud, M. Zeng, M. Popinciuc, G. Güntherodt, B. Beschoten, and B. Özyilmaz, Observation of Long Spin-Relaxation Times in Bilayer Graphene at Room Temperature, Phys. Rev. Lett. **107**, 047206 (2011).

[14] W. Han and R. K. Kawakami, Spin Relaxation in Single-Layer and Bilayer Graphene, Phys. Rev. Lett. **107**, 047207 (2011).

[15] I. Appelbaum, B. Huang, and D. J. Monsma, Electronic measurement and control of spin transport in silicon, Nature (London) **447**, 295 (2007).

[16] B. Huang, D. J. Monsma, and I. Appelbaum, Coherent Spin Transport through a 350 Micron Thick Silicon Wafer, Phys. Rev. Lett. **99**, 177209 (2007).

[17] T. Sasaki, Y. Ando, M. Kameno, T. Tahara, H. Koike, T. Oikawa, T. Suzuki, and M. Shiraishi, Spin Transport in Nondegenerate Si with a Spin MOSFET Structure at Room Temperature, Phys. Rev. Appl. **2**, 034005 (2014).

[18] M. Ishikawa, T. Oka, Y. Fujita, H. Sugiyama, Y. Saito, and K. Hamaya, Spin relaxation through lateral spin transport in heavily doped *n*-type silicon, Phys. Rev. B **95**, 115302 (2017).

[19] R. Jansen, A. Spiesser, H. Saito, Y. Fujita, S. Yamada, K. Hamaya, and S. Yuasa, Nonlinear Electrical Spin Conversion in a Biased Ferromagnetic Tunnel Contact, Phys. Rev. Appl. **10**, 064050 (2018).

[20] C. Cerqueira *et al.*, Evidence of pure spin-current generated by spin pumping in interface-localized states in hybrid metal-silicon-metal vertical structures, Nano Lett. **19**, 90 (2019).

[21] Y. Zhou, W. Han, L.-T. Chang, F. Xiu, M. Wang, M. Oehme, I. A. Fischer, J. Schulze, R. K. Kawakami, and K. L. Wang, Electrical spin injection and transport in germanium, Phys. Rev. B **84,** 125323 (2011).

[22] A. Jain *et al.*, Crossover from Spin Accumulation into Interface States to Spin Injection in the Germanium Conduction Band, Phys. Rev. Lett. **109,** 106603 (2012).

[23] S. Dushenko, M. Koike, Y. Ando, T. Shinjo, M. Myronov, and M. Shiraishi, Experimental Demonstration of Room-Temperature Spin Transport in *n*-Type Germanium Epilayers, Phys. Rev. Lett. **114,** 196602 (2015).

[24] Y. Fujita, M. Yamada, S. Yamada, T. Kanashima, K. Sawano, and K. Hamaya, Temperature-independent spin relaxation in heavily doped *n*-type germanium, Phys. Rev. B **94,** 245302 (2016).

[25] Y. Fujita, M. Yamada, M. Tsukahara, T. Oka, S. Yamada, T. Kanashima, K. Sawano, and K. Hamaya, Spin Transport and Relaxation up to 250 K in Heavily Doped *n*-Type Ge Detected Using $Co_2FeAl_{0.5}Si_{0.5}$ Electrodes, Phys. Rev. Appl. **8,** 014007 (2017).

[26] J. L. Cheng, M. W. Wu, and J. Fabian, Theory of the Spin Relaxation of Conduction Electrons in Silicon, Phys. Rev. Lett. **104,** 016601 (2010).

[27] P. Li and H. Dery, Spin-Orbit Symmetries of Conduction Electrons in Silicon, Phys. Rev. Lett. **107,** 107203 (2011).

[28] Y. Song and H. Dery, Analysis of phonon-induced spin relaxation processes in silicon, Phys. Rev. B **86,** 085201 (2012).

[29] J.-M. Tang, B. T. Collins, and M. E. Flatté, Electron spin-phonon interaction symmetries and tunable spin relaxation in silicon and germanium, Phys. Rev. B **85,** 045202 (2012).

[30] P. Li, Y. Song, and H. Dery, Intrinsic spin lifetime of conduction electrons in germanium, Phys. Rev. B **86,** 085202 (2012).

[31] P. Li, J. Li, L. Qing, H. Dery, and I. Appelbaum, Anisotropy-Driven Spin Relaxation in Germanium, Phys. Rev. Lett. **111,** 257204 (2013).

[32] E. J. Loren, J. Rioux, C. Lange, J. E. Sipe, H. M. van Driel, and A. L. Smirl, Hole spin relaxation and intervalley electron scattering in germanium, Phys. Rev. B **84,** 214307 (2011).

[33] C. Guite and V. Venkataraman, Temperature dependence of spin lifetime of conduction electrons in bulk germanium, Appl. Phys. Lett. **101,** 252404 (2012).

[34] F. Pezzoli, F. Bottegoni, D. Trivedi, F. Ciccacci, A. Giorgioni, P. Li, S. Cecchi, E. Grilli, Y. Song, M. Guzzi, H. Dery, and G. Isella, Optical Spin Injection and Spin Lifetime in Ge Heterostructures, Phys. Rev. Lett. **108,** 156603 (2012).

[35] A. Giorgioni, E. Vitiello, E. Grilli, M. Guzzi, and F. Pezzoli, Valley-dependent spin polarization and long-lived electron spins in germanium, Appl. Phys. Lett. **105,** 152404 (2014).

[36] C. Zucchetti, F. Bottegoni, C. Vergnaud, F. Ciccacci, G. Isella, L. Ghirardini, M. Celebrano, F. Rortais, A. Ferrari, A. Marty, M. Finazzi, and M. Jamet, Imaging spin diffusion in germanium at room temperature, Phys. Rev. B **96,** 014403 (2017).

[37] S. De Cesari, A. Balocchi, E. Vitiello, P. Jahandar, E. Grilli, T. Amand, X. Marie, M. Myronov, and F. Pezzoli, Spin-coherent dynamics and carrier lifetime in strained $Ge_{1-x}Sn_x$ semiconductors on silicon, Phys. Rev. B **99,** 035202 (2019).

[38] Y. Song, O. Chalaev, and H. Dery, Donor-Driven Spin Relaxation in Multivalley Semiconductors, Phys. Rev. Lett. **113,** 167201 (2014).

[39] S. Sato, M. Ichihara, M. Tanaka, and R. Nakane, Electron spin and momentum lifetimes in two-dimensional Si accumulation channels: Demonstration of Schottky-barrier spin metal-oxide-semiconductor field-effect transistors at room temperature, Phys. Rev. B **99,** 165301 (2019).

[40] M. Yamada, Y. Fujita, M. Tsukahara, S. Yamada, K. Sawano, and K. Hamaya, Large impact of impurity concentration on spin transport in degenerate *n*-Ge, Phys. Rev. B **95,** 161304(R) (2017).

[41] O. Chalaev, Y. Song, and H. Dary, Suppressing the spin relaxation of electrons in silicon, Phys. Rev. B **95,** 035204 (2017).

[42] R. People, Indirect band gap of coherently strained Ge_xSi_{1-x} bulk alloys on $\langle 001 \rangle$ silicon substrates, Phys. Rev. B **32,** 1405R (1985).

[43] S. Krishnamurthy, A. Sher, and A.-B. Chen, Band structures of Si_xGe_{1-x} alloys, Phys. Rev. B **33,** 1026 (1986).

[44] M. V. Fischetti and S. E. Laux, Band structure, deformation potentials, and carrier mobility in strained Si, Ge, and SiGe alloys, J. Appl. Phys. **80,** 2234 (1996).

[45] T. Naito, M. Yamada, M. Tsukahara, S. Yamada, K. Sawano, and K. Hamaya, Pure spin current transport in a SiGe alloy, Appl. Phys. Express **11,** 053006 (2018).

[46] H.-C. Luan, D. R. Lim, K. K. Lee, K. M. Chen, J. G. Sandland, K. Wada, and L. C. Kimerling, High-quality Ge epilayers on Si with low threading-dislocation densities, Appl. Phys. Lett. **75,** 2909 (1999).

[47] K. Sawano, Y. Hoshi, S. Kubo, K. Arimoto, J. Yamanaka, K. Nakagawa, K. Hamaya, M. Miyao, and Y. Shiraki, Structural and electrical properties of Ge(111) films grown on Si(111) substrates and application to Ge(111)-on-insulator, Thin Solid Films **613,** 24 (2016).

[48] M. Yamada, K. Sawano, M. Uematsu, and K. M. Itoh, Suppression of surface segregation of the phosphorous δ-doping layer by insertion of an ultra-thin silicon layer for ultra-shallow Ohmic contacts on *n*-type germanium, Appl. Phys. Lett. **107,** 132101 (2015).

[49] M. Yamada, T. Naito, M. Tsukahara, S. Yamada, K. Sawano, and K. Hamaya, Observation of local magnetoresistance signals in a SiGe-based lateral spin-valve device, Semicond. Sci. Technol. **33,** 114009 (2018).

[50] Q. M. Ma and K. L. Wang, Strain-induced nonlinear energy-band splitting of $Si_{1-x}Ge_x$ alloys coherently grown on (111) and (110) oriented Ge substrates, Appl. Phys. Lett. **58,** 1184 (1991).

[51] R. Vrijen, E. Yablonovitch, K. Wang, H. W. Jiang, A. Balandin, V. Roychowdhury, T. Mor, and D. DiVincenzo, Electron-spin-resonance transistors for quantum computing in silicon-germanium heterostructures, Phys. Rev. A **62,** 012306 (2000).

[52] D. J. Paul, Si/SiGe heterostructures: From material and physics to devices and circuits, Semicond. Sci. Technol. **19,** R75 (2004).

[53] M. L. Lee, E. A. Fitzgerald, M. T. Bulsara, M. T. Currie, and A. Lochtefeld, Strained Si, SiGe, and

Ge channels for high-mobility metal-oxide-semiconductor field-effect transistors, J. Appl. Phys. **97,** 011101 (2005).

[54] Y.-J. Yang, W. S. Ho, C.-F. Huang, S. T. Chang, and C. W. Liu, Electron mobility enhancement in strained-germanium *n*-channel metal-oxide-semiconductor field-effect transistors, Appl. Phys. Lett. **91,** 102103 (2007).

[55] Y. Fujita, M. Yamada, M. Tsukahara, T. Naito, S. Yamada, K. Sawano, and K. Hamaya, Nonmonotonic bias dependence of local spin accumulation signals in ferromagnet/semiconductor lateral spin-valve devices, Phys. Rev. B **100,** 024431 (2019).

[56] R. Shan, H. Sukegawa, W. H. Wang, M. Kodzuka, T. Furubayashi, T. Ohkubo, S. Mitani, K. Inomata, and K. Hono, Demonstration of Half-Metallicity in Fermi-Level-Tuned Heusler Alloy $Co_2FeAl_{0.5}Si_{0.5}$ at Room Temperature, Phys. Rev. Lett. **102,** 246601 (2009).

[57] R. Farshchi and M. Ramsteiner, Spin injection from Heusler alloys into semiconductors: A materials perspective, J. Appl. Phys. **113,** 191101 (2013).

[58] M. Johnson and R. H. Silsbee, Interfacial Charge-Spin Coupling: Injection and Detection of Spin Magnetization in Metals, Phys. Rev. Lett. **55,** 1790 (1985).

[59] F. J. Jedema, H. B. Heersche, A. T. Filip, J. J. A. Baselmans, and B. J. van Wees, Electrical detection of spin precession in a metallic mesoscopic spin valve, Nature (London) **416,** 713 (2002).

[60] If the intervalley scattering was completely suppressed and conduction electrons populated only in the lowest energy *L* valley, we should use $g \sim 0.82$. As discussed later, however, the spin lifetimes estimated did not show the complete suppression of the intervalley scattering because of the insufficient strain-induced valley splitting and of the high E_F in the heavily doped $Si_{0.1}Ge_{0.9}$. In short, since we assumed that the suppression of the intervalley scattering is partial, we used $g = 1.56$ which is the average value of all the 4 *L* valleys.

[61] L. O'Brien, D. Spivak, N. Krueger, T. A. Peterson, M. J. Erickson, B. Bolon, C. C. Geppert, C. Leighton, and P. A. Crowell, Observation and modelling of ferromagnetic

[62] contact-induced spin relaxation in Hanle spin precession measurements, Phys. Rev. B **94,** 094431 (2016).

[62] D. K. Wilson, Electron spin resonance experiments on shallow donors in germanium, Phys. Rev. **134,** A265 (1964).

[63] W. G. Spitzer, F. A. Trumbore, and R. A. Logan, Properties of heavily doped *n*-type germanium, J. Appl. Phys. **32,** 1822 (1961).

[64] J. H. Reuszer and P. Fisher, An optical determination of the ground-state splittings of group V impurities in germanium, Phys. Rev. **135,** A1125 (1964).

[65] M. H. Zoellner, M.-I. Richard, G. A. Chahine, P. Zaumseil, C. Reich, G. Capellini, F. Montalenti, A. Marzegalli, Y.-H. Xie, T. U. Schülli, M. Häberlen, P. Storck, and T. Schroeder, Imaging structure and composition homogeneity of 300 mm SiGe virtual substrates for advanced CMOS applications by scanning X-ray diffraction microscopy, ACS Appl. Mater. Interfaces **7,** 9031 (2015).

[66] K. Shida, S. Takeuchi, Y. Imai, S. Kimura, A. Schulze, M. Caymax, and A. Sakai, Tomographic mapping analysis in the depth direction of high-Ge-content SiGe layers with compositionally graded buffers using nanobeam X-ray diffraction, ACS Appl. Mater. Interfaces **9,** 13726 (2017).

[67] K. Shida, S. Takeuchi, T. Tohei, Y. Imai, S. Kimura, A. Schulze, M. Caymax, and A. Sakai, Depth-resolved analysis of lattice distortions in high-Ge-content SiGe/compositionally graded SiGe films using nanobeam x-ray diffraction, Semicond. Sci. Technol. **33,** 124005 (2018).

[68] M. Yamada, M. Tsukahara, Y. Fujita, T. Naito, S. Yamada, K. Sawano, and K. Hamaya, Room-temperature spin transport in *n*-Ge probed by four-terminal nonlocal measurements, Appl. Phys. Express **10,** 093001 (2017).

[69] S. R. Mehrotra, A. Paul, and G. Klimeck, Atomistic approach to alloy scattering in $Si_{1-x}Ge_x$, Appl. Phys. Lett. **98,** 173503 (2011).

[70] Because Si_xGe_{1-x} are not ordered alloys but random solid-solution alloys, one generally does not have to consider the influence of the broken inversion symmetry in the crystal structure on the spin lifetime. In future, however, further relevant studies on the spin relaxation mechanism in Si_xGe_{1-x} alloys should be conducted to verify it.